frontiers in Materials

ORIGINAL RESEARCH
published: 16 December 2020
doi: 10.3389/fmats.2020.577867

Constitutive Modeling of the Flow Stress Behavior for the Hot Deformation of Cu-15Ni-8Sn Alloys

Dongxin Niu[1], *Chao Zhao*[1], *Daoxi Li*[1], *Zhi Wang*[1,2], *Zongqiang Luo*[1,2] *and Weiwen Zhang*[1,2]*

[1]*Guangdong Key Laboratory for Processing and Forming of Advanced Metallic Materials, South China University of Technology, Guangzhou, China,* [2]*School of Mechanical and Automotive Engineering, South China University of Technology, Guangzhou, China*

Three constitutive models, strain-compensated Arrhenius model, modified Johnson–Cook (JC) model, and modified Zerilli–Armstrong (ZA) model, were established for the hot-deformed Cu-15Ni-8Sn alloy based on hot compression tests. By introducing average absolute relative error (AARE), correlation coefficient (R), and relative error, the prediction accuracy of these three models was assessed. The results indicate that strain-compensated Arrhenius model has the highest accuracy at describing the flow stress behavior of the studied alloy, followed by modified JC model and modified ZA model. Moreover, the strain-compensated Arrhenius model established in this work has a great practicability in the hot-extrusion simulation of Cu-15Ni-8Sn alloys. This article provides a theoretical basis for optimizing hot deformation parameters in industrial production of the Cu-15Ni-8Sn alloys.

Keywords: Cu-15Ni-8Sn alloy, hot deformation, flow stress behavior, constitutive models, simulation

OPEN ACCESS

Edited by:
Massimiliano Fraldi,
University of Naples Federico II, Italy

Reviewed by:
Qiao Yanxin,
Jiangsu University of Science and Technology, China
Jianan Hu,
Independent Researcher, Guildford, United Kingdom

***Correspondence:**
Weiwen Zhang
mewzhang@scut.edu.cn

Specialty section:
This article was submitted to Mechanics of Materials, a section of the journal Frontiers in Materials.

Received: *30 June 2020*
Accepted: *06 November 2020*
Published: *16 December 2020*

Citation:
Niu D, Zhao C, Li D, Wang Z, Luo Z and Zhang W (2020) Constitutive Modeling of the Flow Stress Behavior for the Hot Deformation of Cu-15Ni-8Sn Alloys. Front. Mater. 7:577867. doi: 10.3389/fmats.2020.577867

INTRODUCTION

As an attractive substitute for Cu-Be alloys, Cu-15Ni-8Sn alloys have drawn more and more attention owing to their high mechanical strength, excellent wear resistance, and corrosion resistance (Zhang et al., 2017b; Jiang et al., 2019; Cheng et al., 2020; Singh et al., 2007). They are expected to be widely used in aerospace, mechanical systems, and electronic industry (Li et al., 2017; Wang et al., 2019). Along with the research progress on Cu-15Ni-8Sn alloys, the industrialized production of these alloys has been given more and more attention. Most metallic materials underwent at least one of the deformation processes, such as rolling, forging, and extrusion. These processes not only decide materials' final or near-net shapes, but also effectively reduce cast defects, such as porosities and slag inclusions (Cribb et al., 2013; Luo et al., 2019). Moreover, as-cast Cu-15Ni-8Sn alloy ingots usually need a long time homogenization treatment due to inevitably inverse segregation of Sn, where the large-sized grains will be obtained. Therefore, hot deformation process was usually used to refine the grain size and eliminate cast defects, which plays an important role in improving the mechanical properties of these alloys. Many previous researches have shown that the hot deformation parameters have a significant impact on alloy's microstructure and properties. Zhao et al. (2017; 2020) reported that increasing extrusion ratio of Cu-15Ni-8Sn alloys can refine grains and increase recrystallization percentage, which effectively improves the elongation and strength. Thus, it has great significance in optimizing these parameters for achieving optimized properties in industrial productions. The constitutive models have been widely used to predict flow stress, which have high prediction accuracy, and hence they are essential for optimizing the hot deformation parameters of Cu-15Ni-8Sn alloy.

TABLE 1 | Chemical compositions of the alloy (wt%).

Ni	Sn	Si	Ti	Cu
15.23	7.92	0.29	0.09	Bal.

Nowadays, many constitutive models have been proposed and modified to describe the hot deformation behavior of metallic materials under given loading conditions (He et al., 2008; Lin et al., 2009). Among these models, modified Johnson–Cook (JC) model (Umbrello et al., 2007; Grujicic et al., 2012), strain-compensated Arrhenius model (Kumar et al., 2018), and modified Zerilli–Armstrong (ZA) model (Zerilli and Armstrong, 1987) have been widely used. However, for different materials, the most suitable model is usually different. Rudra et al. (2019) compared the three models' accuracy for Al-10%SiCp composite and concluded that modified ZA model is the most suitable compared to the other two models. Yang et al. (2020) investigated the constitutive model of TC17 alloys and found that strain-compensated Arrhenius model has a good agreement with the experimental results. Even for the same Cu-based alloys, different alloy elements can lead to different suitable constitutive models. Zhang et al. (2017a) studied the hot deformation behavior of Cu-Cr-Nb alloys and established a strain-compensated Arrhenius model with high accuracy. But that is m-JC model for Cu-Zn-Si alloys (Wang et al., 2003). Nowadays, there is no work reporting the suitable constitutive model for Cu-15Ni-8Sn alloy which is crucial for prediction and tuning their microstructure and mechanical properties during industrialization. The previous constitutive models for other Cu alloys might shed light on the hot deformation of Cu-15Ni-8Sn alloys. However, a full and precise answer is needed since Cu-15Ni-8Sn alloys show much different microstructure, phase stability, and recrystallization behavior with other Cu alloys such as Cu-Cr-Nb alloys. It is useful for finding the appropriate hot deformation process.

In this work, the constitutive models for the hot-deformed Cu-15Ni-8Sn alloy were built based on strain-compensated Arrhenius model, modified JC model, and modified ZA model. The accuracy of these models was assessed by average absolute relative errors (AARE), correlation coefficient (R), and relative error. Furthermore, the model's practicability in hot-extrusion simulation of Cu-15Ni-8Sn alloys has been evaluated.

MATERIALS AND EXPERIMENTAL DETAILS

The ingots with a designed composition of Cu-15Ni-8Sn-0.3Si-0.1Ti (wt%) were prepared using high purity Cu, Ni, Sn, Si, and Ti in intermediate frequency induction furnace. Minor addition of Si and Ti is usually used in these alloys to refine grains and improve mechanical proprieties. The actual chemical components of the ingot are listed in **Table 1**. The ingots underwent homogenization treatment at 1,113 K for 8 h. Subsequently, a number of ingots were machined into the cylindrical specimens with a size of Φ8 mm×12 mm for compression tests, and the remaining ingots were machined to cylindrical specimens with a size of Φ50 mm × 50 mm for hot-extrusion experiments.

Compression tests were carried out on Gleeble-3500 thermal simulator under different temperatures (1,023, 1,073, 1,123, and 1,173 K) and different strain rates (0.001, 0.01, 0.1, 1, and 10 s^{-1}) with a total strain of 0.9. The detailed results of compression tests were shown in our previous works (Zhao et al., 2019). Based on the hot compression test, the flow stress data obtained in the strain range of 0.1–0.9 at intervals of 0.1 were used to calibrate constitutive models, and the compression stress data obtained in the strain range of 0.1–0.9 at intervals of 0.05 were used to validate the model.

Hot extrusion was carried out on a 2,000 KN vertical extruding machine, and then the samples were naturally cooled to room temperature in air. The detailed extrusion parameters are listed in **Table 2**. The OM images were obtained with a LEICA/DMI 5,000 M optical microscope. The grain size distribution map was drawn from more than 50 random areas based on the observation of OM images, and the average grain size was measured according to the linear-intercept method using an image analysis software installed on the Leica materials workstation.

CONSTITUTIVE MODELING

Strain-Compensated Arrhenius Model (sc-Arrhenius Model)

The Arrhenius model is usually used to describe the material hot deformation behavior, which can be expressed as **Eqs. 1–3** (Kumar et al., 2018):

$$\dot{\varepsilon} = A_1 + \sigma^{n_1} exp\left(-\frac{Q}{RT}\right), \quad \alpha\sigma < 0.8, \tag{1}$$

$$\dot{\varepsilon} = A_2 exp\,(n_2\sigma) exp\left(-\frac{Q}{RT}\right), \quad \alpha\sigma > 1.2, \tag{2}$$

$$\dot{\varepsilon} = A\,[\sinh\,(\alpha\sigma)]^n exp\left(-\frac{Q}{RT}\right), \quad \text{for all } \alpha\sigma, \tag{3}$$

where $\dot{\varepsilon}$ is the strain rate; σ is the flow stress; A_1, A_2, A, n_1, n_2, n, and α are the material constants; Q is the activation energy in hot deformation process; and R is the universal gas constant (8.314 J/mol/K).

By taking natural logarithm form to **Eqs. 1–3**, the following equations can be obtained:

$$\ln\dot{\varepsilon} = lnA_1 + n_1 ln\sigma - \frac{Q}{RT}, \tag{4}$$

$$\ln\dot{\varepsilon} = lnA_2 + n_2\sigma - \frac{Q}{RT}, \tag{5}$$

$$\ln\dot{\varepsilon} = lnA + nln\,[\sinh\,(\alpha\sigma)] - \frac{Q}{RT}, \tag{6}$$

where n_1, n_2, and n can be calculated from the slop of fitting curves $\ln\dot{\varepsilon} - ln\sigma$, $\ln\dot{\varepsilon} - \sigma$, and $\ln\dot{\varepsilon} - ln\,[sinh\,(\alpha\sigma)]$, respectively, and the value of α can be obtained, which is defined as n_2/n_1. From **Eq. 6**, the value of lnA is equal to the intercept of fitting curve: $ln\,[\sinh\,(\alpha\sigma)] - \left(\ln\dot{\varepsilon} + \frac{Q}{RT}\right) - \left(\ln\dot{\varepsilon} + \frac{Q}{RT}\right)$.

TABLE 2 | The hot-extrusion parameters.

Diameter of sample (mm)	Diameter of extrusion bar (mm)	Extrusion ratio	Extrusion temperature (K)	Extrusion speed (mm/s)
50	12	17	1,173	3

TABLE 3 | Coefficient of polynomial for α, lnA, n, and Q.

α	n	Q (kJ/mol)	lnA
B_0 = 0.00949	C_0 = 3.79115	D_0 = 269.39728	E_0 = 26.30386
B_1 = −0.01936	C_1 = −2.3695	D_1 = −31.85674	E_1 = 1.59392
B_2 = 0.1278	C_2 = 15.84868	D_2 = 1779.71354	E_2 = 152.02558
B_3 = −0.44303	C_3 = −61.29022	D_3 = −9,514.48648	E_3 = −877.72648
B_4 = 0.89522	C_4 = 147.0221	D_4 = 24,689.96146	E_4 = 2,345.69714
B_5 = −1.04129	C_5 = −197.07731	D_5 = −33,891.29419	E_5 = −3,257.9071
B_6 = 0.64334	C_6 = 136.31354	D_6 = 23,645.39175	E_6 = 2,279.9444
B_7 = −0.16254	C_7 = −37.83832	D_7 = −6,558.01348	E_7 = −630.9665
R^2 = 0.96268	R^2 = 0.99389	R^2 = 0.99542	R^2 = 0.99567

By regarding $\dot{\varepsilon}$ as a constant parameter, **Eq. 7** can be obtained from **Eq. 6** with respect to $1/T$. Hence, the value of Q can be calculated by n, R, and S (defined as the slope of fitting curve $1/T - \ln[\sinh(\alpha\sigma)]$).

$$Q = R \times n \times \frac{d\{\ln sinh[(\alpha\sigma)]\}}{d(1/T)} = RnS. \tag{7}$$

However, the strain, which has a significant effect on the flow stress, is not taken into account in Arrhenius model. Here, a strain compensation method, shown as **Eqs. 8–11**, was introduced in this work based on the study reported by Kumar et al. (2018). The different parameter values of α, n, Q, and A at each strain can be calculated following the above-mentioned method. Subsequently, the fitting curve is drawn to obtain the coefficients in **Eqs. 9–12**, and the results are listed in **Table 3**.

$$\alpha = B_0 + B_1\varepsilon + B_2\varepsilon^2 + B_3\varepsilon^3 + B_4\varepsilon^4 + B_5\varepsilon^5 + B_6\varepsilon^6 + B_7\varepsilon^7, \tag{8}$$

$$n = C_0 + C_1\varepsilon + C_2\varepsilon^2 + C_3\varepsilon^3 + C_4\varepsilon^4 + C_5\varepsilon^5 + C_6\varepsilon^6 + C_7\varepsilon^7, \tag{9}$$

$$Q = D_0 + D_1\varepsilon + D_2\varepsilon^2 + D_3\varepsilon^3 + D_4\varepsilon^4 + D_5\varepsilon^5 + D_6\varepsilon^6 + D_7\varepsilon^7, \tag{10}$$

$$lnA = E_0 + E_1\varepsilon + E_2\varepsilon^2 + E_3\varepsilon^3 + E_4\varepsilon^4 + E_5\varepsilon^5 + E_6\varepsilon^6 + E_7\varepsilon^7. \tag{11}$$

Modified Johnson–Cook Model

Modified JC model can be expressed as **Eq. 12** (Grujicic et al., 2012):

$$\sigma = (A_1 + B_1\varepsilon + B_2\varepsilon^2)(1 + C_1 ln\dot{\varepsilon}^*)exp\left[(\lambda_1 + \lambda_2 ln\dot{\varepsilon}^*)(T - T_{ref})\right], \tag{12}$$

where σ is flow stress; ε is true strain; A_1, B_1, B_2, C_1, λ_1, and λ_2 are material constants; $\dot{\varepsilon}^*$ is equal to $\dot{\varepsilon}/\dot{\varepsilon}_0$, where $\dot{\varepsilon}$ is strain rate and $\dot{\varepsilon}_0$ is reference strain rate; T is current temperature; T_{ref} is reference temperature. In this study, $\dot{\varepsilon}_0$ and T_{ref} are considered to be 0.001 s^{-1} and 1,023 K, respectively, which is the lowest strain rate and temperature in hot compression test.

TABLE 4 | Values of the coefficients in modified JC model.

A_1	B_1	B_2	C_1	λ_1	λ_2
68.62711	9.13282	−3.51248	0.3857	−0.00786	0.000413

a. At Reference Strain Rate and Reference Temperature

Equation 12 can be simplified to the following form:

$$\sigma = (A_1 + B_1\varepsilon + B_2\varepsilon^2), \tag{13}$$

where the values of A_1, B_1, and B_2 can be calculated from the fitting curve between ε and σ.

a. At Reference Temperature

Equation 12 can be simplified to the following form:

$$\sigma = (A_1 + B_1\varepsilon + B_2\varepsilon^2)(1 + C_1 ln\dot{\varepsilon}^*), \tag{14}$$

Through drawing the fitting curve $ln\dot{\varepsilon}^* - \sigma/(A_1 + B_1\varepsilon + B_2\varepsilon^2)$, the value of C_1 (equal to the average slope) can be calculated.

a. At Each Strain Rate

A new relationship $\lambda = (\lambda_1 + \lambda_2 ln\dot{\varepsilon}^*)$ is introduced to **Eq. 12**, followed by taking natural logarithm form to obtain the following equation:

$$ln\frac{\sigma}{(A_1 + B_1\varepsilon + B_2\varepsilon^2)(1 + C_1 ln\dot{\varepsilon}^*)} = \lambda\left(T - T_{ref}\right), \tag{15}$$

where the values of λ can be obtained from the fitting curve of $ln\frac{\sigma}{(A_1+B_1\varepsilon+B_2\varepsilon^2)(1+C_1 ln\dot{\varepsilon}^*)}$ and $(T - T_{ref})$. Four different values of λ correspond to four different strain rates. Subsequently, by the fitting curve $ln\dot{\varepsilon}^* - \lambda$, λ_1 (the intercept) and λ_2 (the slope) can be calculated.

The calculated values of the coefficients are listed in **Table 4**.

Modified Zerilli–Armstrong Model

Modified ZA model can be expressed as **Eq. 16** (Samantaray et al., 2011):

$$\sigma = (C_1 + C_2\varepsilon^n)exp\left[-(C_3 + C_4\varepsilon + C_5\varepsilon^2)T^* + (C_6 + C_7T^*)ln\dot{\varepsilon}^*\right], \tag{16}$$

TABLE 5 | Values of the parameters in modified ZA model.

C_1	C_2	n	C_3	C_4	C_5	C_6	C_7
69.323	7.56677	0.85838	0.00698	0.000876	−0.00201	0.1639	0.000311

where C_1, C_2, C_3, C_4, C_5, C_6, C_7, and n are material constants; T^* is equal to $(T - T_{ref})$, where T_{ref} is the reference temperature; $\dot{\varepsilon}^*$ is equal to $\dot{\varepsilon}/\dot{\varepsilon}_0$, where $\dot{\varepsilon}_0$ is the reference strain rate. Similar to that, in modified JC model, the reference strain rate and temperature are also defined as 0.001 s^{-1} and 1,023 K.

a. At Reference Strain Rate

The natural logarithm form is taken to both sides of the equation to obtain the following form. Here, M and N are introduced to the equation to make it clearer.

$$ln\sigma = M - NT^*, \tag{17}$$

$$M = \ln(C_1 + C_2\varepsilon^n), \tag{18}$$

$$N = C_3 + C_4\varepsilon + C_5\varepsilon^2. \tag{19}$$

By drawing fitting curve $T^* - ln\sigma$, the different values of M and N can be obtained under different strains. Subsequently, the fitting curve of ε-M and ε-N can be drawn, from which the values of n, C_2, C_3. C_4, and C_5 can be obtained. Additionally, the value of C_1 is approximately the same as the yield stress at reference temperature and reference strain rate.

a. At Each Strain Rate

The natural logarithm of the modified ZA model is taken to generate the following equation:

$$ln\sigma = ln(C_1 + C_2\varepsilon^n) - \left(C_3 + C_4\varepsilon + C_5\varepsilon^2\right)T^* + (C_6 + C_7T^*)ln\dot{\varepsilon}^*, \tag{20}$$

where four values of $(C_6 + C_7T^*)$ are obtained for four different temperatures from the fitting curve between $ln\dot{\varepsilon}^*$ and $ln\sigma$. After linear fitting of these four sets of data, the values of C_6 and C_7 can be obtained.

The calculated values of the coefficients are listed in **Table 5**.

Comparison of the Constitutive Models

The predictability of the flow stress-strain relationship by the constitutive models is assessed by graphical comparison between the calculated values and the experimental data at varied experimental conditions, as shown in **Figures 1–3**. As shown in **Figure 1**, the flow stress-strain curve, calculated by the sc-Arrhenius model, fits well with the experimental data except the conditions at high temperature of 1,173 K and high strain rate of 10 s^{-1}. Under this condition, the calculated values are higher than the experimental data after the strain of 0.2. Under this condition, an unsteady deformation zone, cracks appear in the specimen, leading to a rapid reduction in flow stress with the strain increasing [19]. Because sc-Arrhenius model is failed to predict the reduction in flow stress contributed by the crack formation, the calculated results are higher than the experimental data at high strain rates.

Figure 2 shows the comparison results of the m-JC model, which indicates that it can only maintain a high predictability at low strain rates. With increasing strain rate (above 0.1 s^{-1}), the predicted results gradually deviate from the experimental data. Additionally, the calculated values of m-JC model are higher than the experimental data after the strain of 0.6, which indicates that m-JC model has low ability to predict the reduction trend in flow stress caused by dynamic recrystallization.

Figure 3 shows the comparison between the experimental and predicted flow stress values obtained by m-ZA model. The m-ZA model's calculation results show a large deviation from experimental data at strain rate above 0.01 s^{-1}, where the predicted values are initially much lower than the experimental data. Moreover, the predicted values constantly increase with increasing strain, which disagrees with the reduction trend of experimental data.

The accuracy of the three models is further verified via employing average absolute relative error (AARE), correlation coefficient (R), and relative error. The R exhibits the linear relationship between experimental and calculated values; the relative error describes the prediction accuracy of a model; and AARE is obtained by term-by-term calculation of relative error. Their expressions are shown as follows (Rudra et al., 2019):

$$AARE = \frac{1}{N}\sum_{i=1}^{N}\left|\frac{E_i - P_i}{E_i}\right|, \tag{21}$$

$$Relative\ error = (E_i - P)/E_i \times 100\%, \tag{22}$$

$$R = \frac{\sum_{i=1}^{i=N}(E_i - \overline{E})(P_i - \overline{P})}{\sqrt{\sum_{i=1}^{i=N}(E_i - \overline{E})^2\sum_{i=1}^{i=N}(P_i - \overline{P})^2}}, \tag{23}$$

where E_i is the experimental value; P_i is the calculated value; $\overline{E}$ and $\overline{P}$ are the mean values of E_i and P_i, respectively; N is the total number of data involved in the calculation.

Figure 4 shows the plots of average absolute relative error, correlation coefficient, and relative error between the calculated values using **Eqs. 20–22** and the experimental data. It can be seen that the sc-Arrhenius model has the highest correlation coefficient of 0.997, followed by m-JC model (0.989) and m-ZA model (0.941), indicating that the calculated values of sc-Arrhenius model have the strongest linearity with experimental data. **Figure 5** shows the distribution of relative errors obtained from the three models. It is found that sc-Arrhenius model shows the highest accuracy with relative error range from −19.932 to 12.541%. Moreover, the relative error values of more than 95% of samples calculated by sc-Arrhenius model are within ±10%. **Table 6** shows the results of AARE calculated by the three models. The sc-Arrhenius model has the lowest value of 0.034, followed by m-JC model (0.075) and m-ZA model (0.098). The results of AARE are in agreement with the results of relative errors. In conclusion, the sc-Arrhenius model possesses the highest prediction accuracy, which shows the highest value of R, lowest value of relative error, and lowest value of AARE.

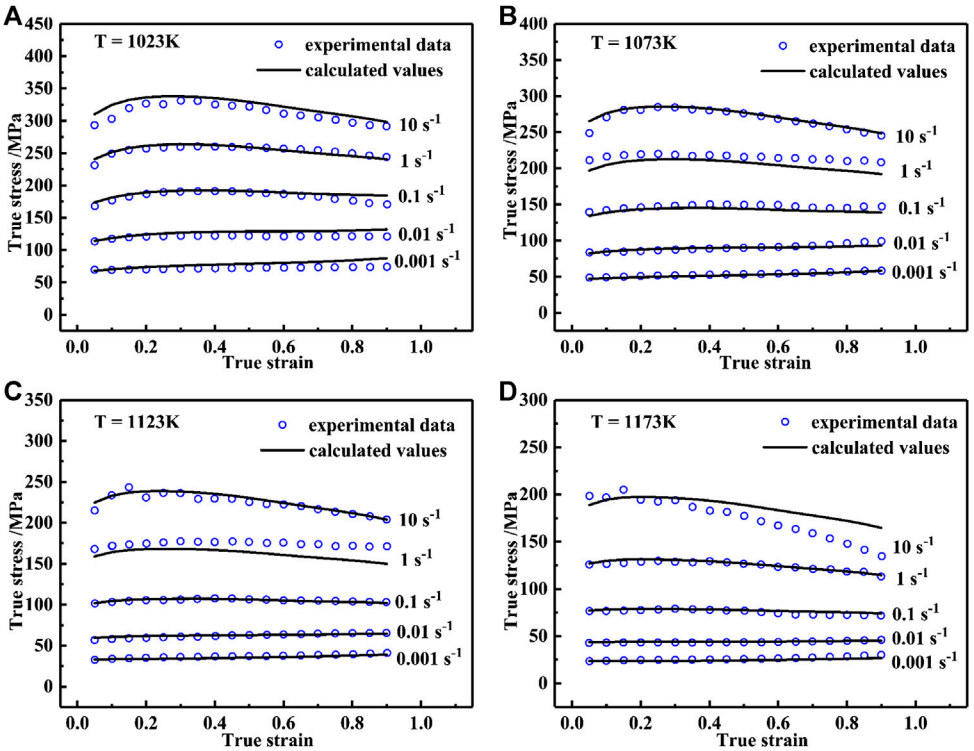

FIGURE 1 | Comparison between experimental data and values calculated by sc-Arrhenius model.

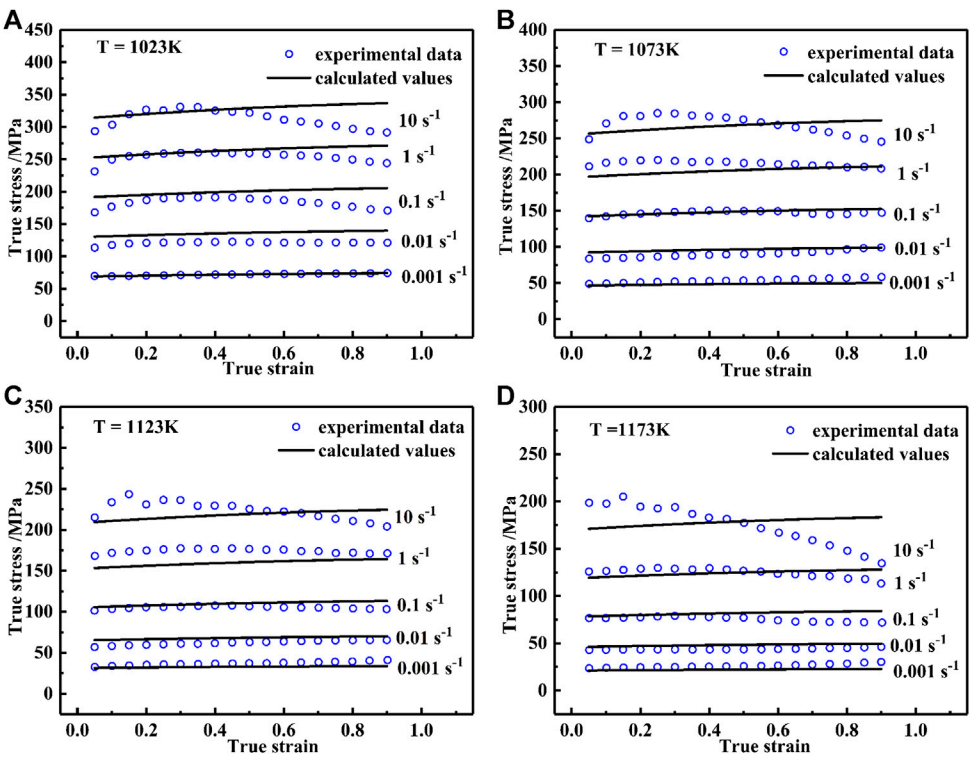

FIGURE 2 | Comparison between experimental data and values calculated by m-JC model.

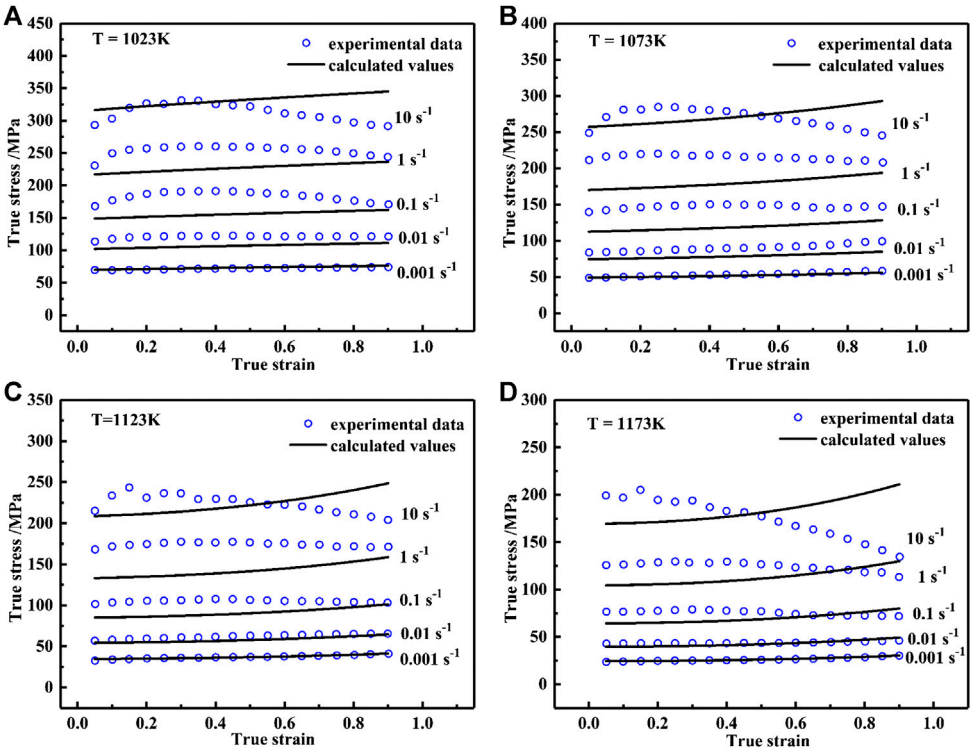

FIGURE 3 | Comparison between experimental data and values calculated by m-ZA model.

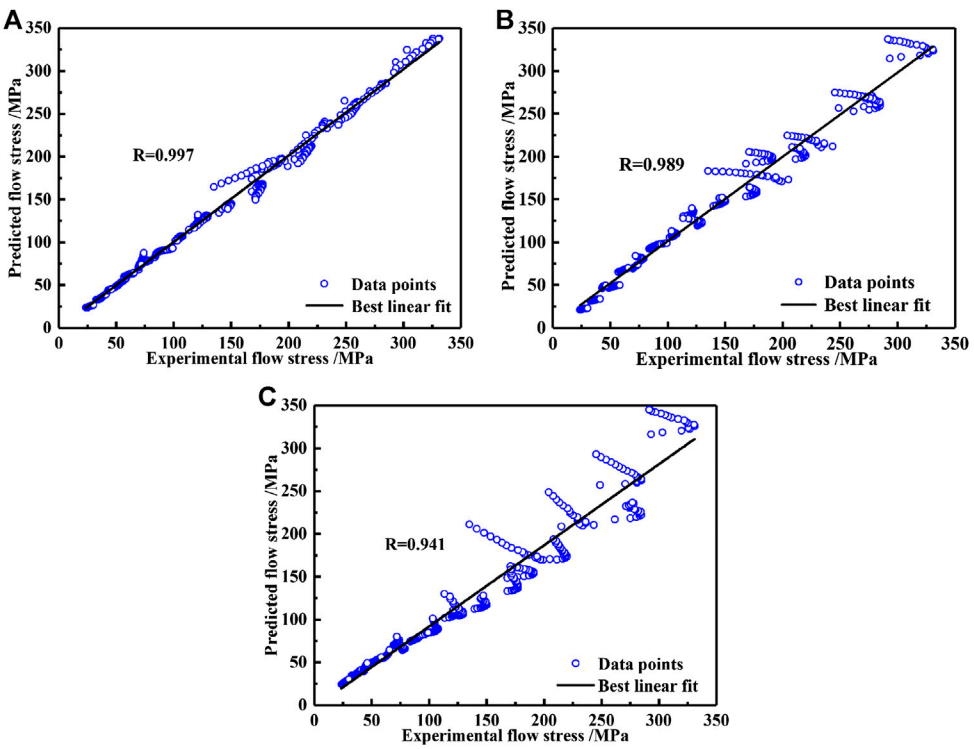

FIGURE 4 | Correlation between experimental and predicted flow stress calculated by **(A)** sc-Arrhenius model; **(B)** m-JC model; **(C)** m-ZA model.

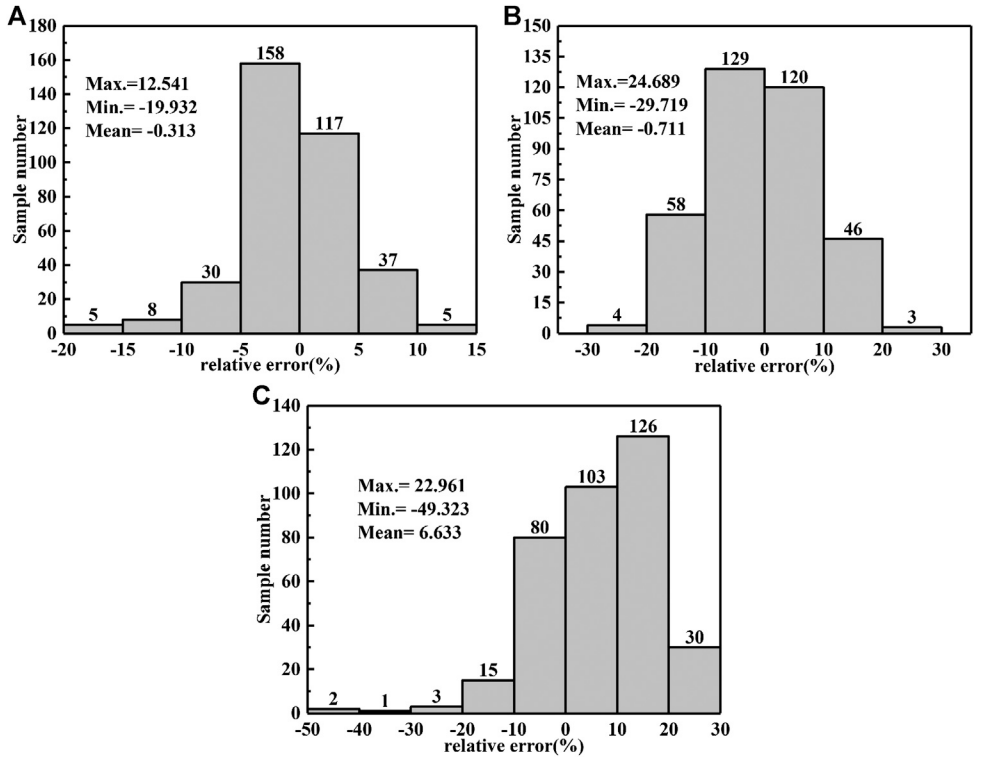

FIGURE 5 | Results of relative errors analysis by using **(A)** sc-Arrhenius model; **(B)** m-JC model; **(C)** m-ZA model.

TABLE 6 | Results of AARE calculated by the three models.

	Strain-compensated Arrhenius	Modified JC	Modified ZA
AARE	0.034	0.075	0.098

The highest prediction accuracy of sc-Arrhenius model could be due to the comprehensive consideration of the strain, strain rate, and temperature. Lennon and Ramesh (2004) pointed out that the effects of temperature, strain, and strain rate are coupled together in FCC metals, and thus considering each term independently is unreasonable. Strain-compensated Arrhenius model takes the coupled effect of strain rate and temperature into consideration by using Z parameter, which is equal to $\dot{\varepsilon} \cdot \exp\left[\frac{Q}{RT}\right]$. A strain compensation method is introduced to estimate the effect of the strain.

As for m-JC model and m-ZA model, the prediction accuracy deteriorates as the strain rate increases. Under the condition of low strain rate (below 0.1 s^{-1}), the prediction results arise from their method of evaluating the effects of temperature, strain, and strain rate. M-JC model only considers the coupled effect of the strain rate and temperature, while the effect of the strain is considered independently. This method fails to describe the weakening of strain hardening caused by restoration process. Thus, the reduction trend in flow stress cannot be described accurately (e.g., at the condition of 1,023 K and 0.1 s^{-1}). Although m-ZA model considers the coupled effect of strain rate and temperature by parameter C_4 and the coupled effect of strain and temperature by parameter C_6 (Samantaray et al., 2009), the predicted flow stress at higher strain rate is still little lower than experimental data. This phenomenon results from the fact that parameters C_2 and n, which relate to strain hardening, are calculated only using the data at reference strain rate. Thus, it fails to predict the strain hardening behavior at higher strain rate. The same phenomenon is also observed in Samantaray et al.'s work (Samantaray et al., 2009; Samantaray et al., 2011). Additionally, under the condition of high strain rate (above 0.1 s^{-1}), the prediction inaccuracy of m-JC model and m-ZA model attributes to the fact that these deformation conditions are located in the unsteady zone of the studied alloys. Our previous study on processing map has pointed out that the unsteady zone is in the range of 1,023–1,198 K and strain rate is greater than 0.6 s^{-1} at a true strain of 0.9 (Zhao et al., 2019). Many cracks were observed in the hot compression specimens tested under these conditions, which are responsible for the decrease of flow stress at high strain rate. However, constitutive models fail to take material instability into account, and the calculated results still increase with the strain because of strain hardening. Owing to this reason, the opposite trend between the predicted and experimental results is observed at high strain rate (above 0.1 s^{-1}).

Practicability of sc-Arrhenius Model

The above results indicate that the constitutive model of sc-Arrhenius model shows the best accuracy for prediction of the

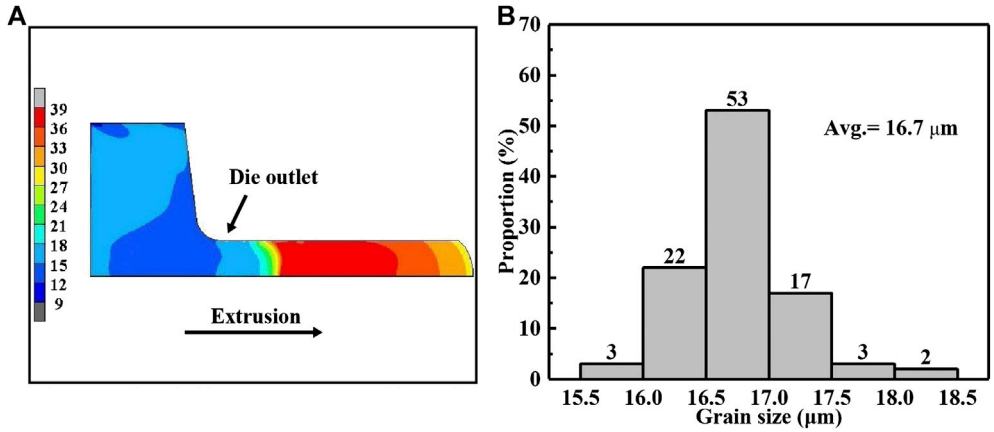

FIGURE 6 | The results of hot-extrusion simulation: **(A)** grain size contour; **(B)** grain size distribution of the bar around die outlet.

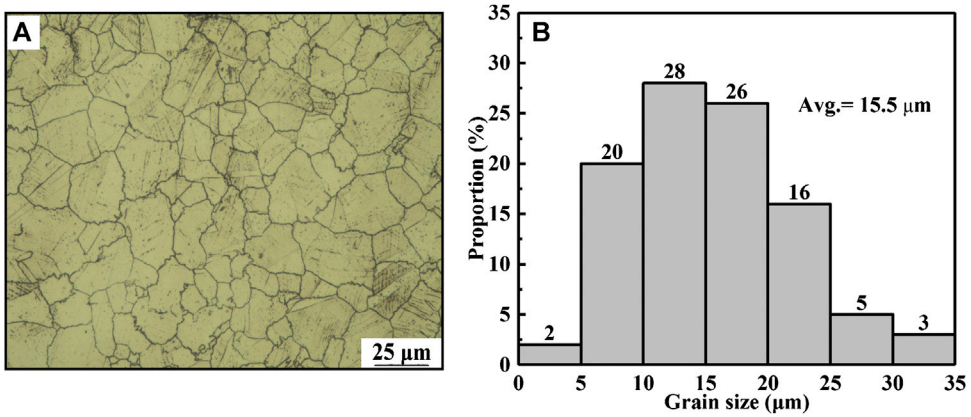

FIGURE 7 | The results of hot-extrusion experiment: **(A)** representative OM image; **(B)** grain size distribution of the bar around die outlet.

flow stress-strain relationship of the hot-deformed Cu-15Ni-8Sn alloy. Here, we further verify the practicability of sc-Arrhenius model in simulation of the hot-extruded Cu-15Ni-8Sn alloy. Usually, for evaluating the practicability of a model, comparing the stress between simulation and experiment is considered as the best method. Given the fact that real-time stress data during the actual extrusion cannot be measured, an indirect method is necessary to be employed to evaluate the practicability. Here, we used finite element analysis (FEA), where the prediction accuracy of temperature, strain, and grain size is all based on the accurate prediction of stress. The accurate simulation of FEA on the basis of Arrhenius model can be considered indirect proof of the practicality of Arrhenius model.

Hot-extrusion experimental methods were described in detail in the above section. Hot-extrusion simulation was performed by using MARC finite element simulation software. Relevant formation parameters are similar to those shown in **Table 2**. The geometric model was established based on experimental methods. The flow stress database, describing the plasticity, was calculated by the sc-Arrhenius model and linked to simulation software. According to the fact that grain size change during hot-extrusion deformation mainly results from dynamic recrystallization (DRX) (Li et al., 2010; Zhao et al., 2017), DRX is taken into account in the simulation. The final result of simulation was obtained using the data at die outlet, after which no DRX exists. As a comparison, the microstructure of extrusion bar around die outlet was studied.

Figure 6A shows the simulated result of the grain size contour. By analyzing simulation data at the position of die outlet, the grain size distribution map is drawn as shown in **Figure 6B**. The predicted average grain size is ~16.7 μm. **Figure 7A** shows a representative OM image obtained from the extrusion bar around die outlet. **Figure 7B** shows the grain size distribution map based on more than 50 random OM images. The average grain size is measured as ~15.5 μm. Comparing the results of simulation and experiment, it can be concluded that sc-Arrhenius model has a great practicability in finite element analysis for hot-deformed Cu-15Ni-8Sn alloys.

CONCLUSION

In this article, the hot compression tests of Cu-15Ni-8Sn alloys at different temperatures from 1,023 to 1,173 K and strain rates from 0.001 to 10 s^{-1} were carried out. Three kinds of constitutive models (sc-Arrhenius model, m-JC model, and m-ZA model) were established and compared with each other. The following conclusions can be drawn:

The strain-compensated Arrhenius model, modified JC model, and modified ZA model of Cu-15Ni-8Sn alloys were established based on hot compression tests, where the sc-Arrhenius model has the highest predictability among the three models. For sc-Arrhenius model, m-JC model, and m-ZA model, the AARE is 0.034, 0.075, and 0.098, respectively, the correlation coefficients are 0.997, 0.989, and 0.941, respectively, and the proportion of samples with relative errors within ±10% is 95, 70, and 51%, respectively.

The practicability of sc-Arrhenius model of the hot-extruded Cu-15Ni-8Sn alloy was verified by performing both simulation and experiment. The simulation and experimental results show similar grain size of 16.7 and 15.5 μm, respectively, indicating that sc-Arrhenius model can accurately predict the flow stress behavior of the hot deformation process of Cu-15Ni-8Sn alloy. This model may provide a theoretical basis for optimization of hot-extrusion parameters.

DATA AVAILABILITY STATEMENT

The raw data supporting the conclusions of this article will be made available by the authors, without undue reservation.

AUTHOR CONTRIBUTIONS

DN, CZ, and DL designed the experiments and conducted the data analysis. ZL and WZ provided the experimental resources and conducted experimental supervision. DN organized the database and wrote the first draft of the manuscript. DN, CZ, ZW, and WZ did the writing-review and editing.

FUNDING

This work was sponsored by the Guangdong Natural Science Foundation for Research Team (Grant No. 2015A030312003) and Guangdong Special Fund Project of Applied Technology Research and Development (Grant No. 2016B090931002).

REFERENCES

Cheng, J. J., Gan, X. P., Li, Z., Lei, Q., and Zhou, K. C. (2020). Wear map for sliding wear behavior of Cu-15Ni-8Sn alloy against bearing steel under oil-lubricated condition. *J. Cent. South Univ.* 27 (2), 311–324. doi:10.1007/s11771-020-4297-y

Cribb, W. R., Gedeon, M. J., and Grensing, F. C. (2013). Performance advances in copper-nickel-tin spinodal alloys. *Adv. Mater. Process.* 171 (9), 23–28. doi:10.1016/j.actamat.2013.07.017

Grujicic, M., Pandurangan, B., Yen, C.-F., and Cheeseman, B. A. (2012). Modifications in the AA5083 johnson-cook material model for use in friction stir welding computational analyses. *J. Mater. Eng. Perform.* 21 (11), 2207–2217. doi:10.1007/s11665-011-0118-7

He, X., Yu, Z., and Lai, X. (2008). A method to predict flow stress considering dynamic recrystallization during hot deformation. *Comput. Mater. Sci.* 44 (2), 760–764. doi:10.1016/j.commatsci.2008.05.021

Jiang, Y. Z., Li, Z., Xiao, Z., Xing, Y., Zhang, Y., and Fang, M. (2019). Microstructure and properties of a Cu-Ni-Sn alloy treated by two-stage thermomechanical processing. *J. Miner. Met. Mater. Soc.* 71 (8), 2734–2741. doi:10.1007/s11837-019-03606-5

Kumar, S., Aashranth, B., Davinci, M. A., Samantaray, D., Borah, U., and Bhaduri, A. K. (2018). Assessing constitutive models for prediction of high-temperature flow behavior with a perspective of alloy development. *J. Mater. Eng. Perform.* 27 (4), 2024–2037. doi:10.1007/s11665-018-3237-6

Lennon, A. M. and Ramesh, K. T. (2004). The influence of crystal structure on the dynamic behavior of materials at high temperatures. *Int. J. Plast.* 20 (2), 269–290. doi:10.1016/s0749-6419(03)00037-8

Li, H., Lu, M., and Luo, J. (2010). "The modulus mensuration of Yada model and the microstructure simulation of casting AZ31 magnesium alloy," in *Manufacturing science and engineering, pts 1-5*. Editors Z. Jiang and C. L. Zhang, 75–80.

Li, Z., Jiang, Y. X., Peng, G. W., and Gan, X. P. (2017). Effect of dynamic strain aging on the deformation behavior and microstructure of cu-15ni-8sn alloy. *J. Alloys Compd.* 718 (2017), 182–187. doi:10.1016/j.jallcom.2017.05.127

Lin, Y.-C., Chen, M.-S., and Zhang, J. (2009). Modeling of flow stress of 42CrMo steel under hot compression. *Mater. Sci. Eng.* 499 (1–2), 88–92. doi:10.1016/j.msea.2007.11.119

Luo, B., Li, D., Zhao, C., Wang, Z., Luo, Z., and Zhang, W. (2019). A low Sn content Cu-Ni-Sn alloy with high strength and good ductility. *Mater. Sci. Eng.* 746, 154–161. doi:10.1016/j.msea.2018.12.120

Rudra, A., Ashiq, M., Das, S., and Dasgupta, R. (2019). Constitutive Modeling for Predicting High-Temperature Flow Behavior in Aluminum 5083+10 Wt Pct SiCp Composite. *Metall. Mater. Trans. B* 50 (2), 1060–1076. doi:10.1007/s11663-019-01531-1

Samantaray, D., Mandal, S., Borah, U., Bhaduri, A. K., and Sivaprasad, P. V. (2009). A thermo-viscoplastic constitutive model to predict elevated-temperature flow behaviour in a titanium-modified austenitic stainless steel. *Mater. Sci. Eng.* 526 (1–2), 1–6. doi:10.1016/j.msea.2009.08.009

Samantaray, D., Mandal, S., Phaniraj, C., and Bhaduri, A. K. (2011). Flow behavior and microstructural evolution during hot deformation of AISI Type 316 L(N) austenitic stainless steel. *Mater. Sci. Eng.* 528 (29–30), 8565–8572. doi:10.1016/j.msea.2011.08.012

Singh, J. B., Cai, W., and Bellon, P. (2007). Dry sliding of Cu-15 wt%Ni-8 wt%Sn bronze: wear behaviour and micro structures. *Wear* 263, 830–841. doi:10.1016/j.wear.2007.01.061

Umbrello, D., M'Saoubi, R., and Outeiro, J. C. (2007). The influence of Johnson-Cook material constants on finite element simulation of machining of AISI 316L steel. *Int. J. Mach. Tool Manufact.* 47 (3–4), 462–470. doi:10.1016/j.ijmachtools.2006.06.006

Wang, J. B., Zhou, X. L., Li, J., Brochu, M., and Zhao, Y. F. (2020). Microstructures and properties of slm-manufactured Cu-15Ni-8Sn alloy. *Addit. Manuf.* 31, 100921. doi:10.1016/j.addma.2019.100921

Wang, Y., Zhou, Y. X., and Xia, Y. M. (2003). A constitutive description of tensile behavior for brass over a wide range of strain rates. *Mater. Sci. Eng.* 372, 186–190. doi:10.1016/j.msea.2003.12.00

Yang, X. K., Wang, K. S., Zhang, Z. J., Guo, M., Cai, J., and Yang, Q. X. (2020). Flow stress prediction for as-cast TC17 titanium alloy. *Rare Met. Mater. Eng.* 49 (4), 1131–1139.

Zerilli, F. J. and Armstrong, R. W. (1987). Dislocation-mechanics-based constitutive relations for material dynamics calculations. *J. Appl. Phys.* 61 (5), 1816–1825. doi:10.1063/1.338024

Zhang, Y., Sun, H., Volinsky, A. A., Tian, B., Song, K., Wang, B., et al. (2017a). Hot workability and constitutive model of the Cu-Zr-Nd alloy. *Vacuum* 146, 35–43. doi:10.1016/j.vacuum.2017.09.017

Zhang, Y., Xiao, Z., Zhao, Y., Li, Z., Xing, Y., and Zhou, K. (2017b). Effect of thermo-mechanical treatments on corrosion behavior of Cu-15Ni-8Sn alloy in 3.5 wt% NaCl solution. *Mater. Chem. Phys.* 199, 54–66. doi:10.1016/j.matchemphys.2017.06.041

Zhao, C., Wang, X., Yu, Y. G., Luo, Z. Q., and Zhang, W. W. (2017). Microstructure evolution of hot-extruded Cu-15Ni-8Sn alloy with different extrusion ratios. *Mater. Sci. Forum* 898, 1140–1147. doi:10.4028/www.scientific.net/MSF.898.1140

Zhao, C., Wang, Z., Li, D., Pan, D., Lou, B., Luo, Z., et al. (2020). Optimization of strength and ductility in an as-extruded Cu-15Ni-8Sn alloy by the additions of Si and Ti. *J. Alloys Compd.* 823, 153759. doi:10.1016/j.jallcom.2020.153759

Zhao, C., Wang, Z., Pan, D.-q., Li, D.-x., Luo, Z.-q., Zhang, D.-t., et al. (2019). Effect of Si and Ti on dynamic recrystallization of high-performance Cu-15Ni-8Sn alloy during hot deformation. *Trans. Nonferrous Metals Soc. China* 29 (12), 2556–2565. doi:10.1016/s1003-6326(19)65163-0

Conflict of Interest: The authors declare that the research was conducted in the absence of any commercial or financial relationships that could be construed as a potential conflict of interest.